NANOSYSTEMS:
PHYSICS, CHEMISTRY, MATHEMATICS

Zamyatina E.A., et al. *Nanosystems: Phys. Chem. Math.*, 2024, **15** (5), 683–692.
http://nanojournal.ifmo.ru

Original article

DOI 10.17586/2220-8054-2024-15-5-683-692

Physicochemical properties and biological activity of novel cerium oxide nanoparticles modified with pyrroloquinoline quinone

Elizaveta A. Zamyatina[1,a], Olga A. Goryacheva[2,b], Nelli R. Popova[1,c]

[1]Institute of Theoretical and Experimental Biophysics of the Russian Academy of Sciences, Pushchino, Russia
[2]Saratov State University named after N. G. Chernyshevsky, Chemistry Institute, Saratov, Russia

[a]sonyoru162@gmail.com, [b]olga.goryacheva.93@mail.ru, [c]nellipopovaran@gmail.com

Corresponding author: Nelli R. Popova, nellipopovaran@gmail.com

ABSTRACT Nanoscale cerium oxide (CeO_2) is a bioavailable inorganic nanozyme exhibiting pronounced redox activity and capable of acting as a delivery system for bioactive compounds. We have synthesized and characterized novel CeO_2 nanoparticles modified with pyrroloquinoline quinone (CeO_2@PQQ). TEM analysis revealed the diameter of the CeO_2@PQQ NPs to be approximately 4 nm, with a hydrodynamic diameter of 62 nm (DLS). Furthermore, the zeta potential was found to be -38 mV (ELS), and FTIR analysis confirmed the adsorption of PQQ on the surface of CeO_2 NPs. The results demonstrated that CeO_2@PQQ NPs exhibited no cytotoxic effects on L929 cells within the concentration range of 0.1 – 10 μM and did not adversely affect the mitochondrial function of the cells. It was demonstrated that CeO_2@PQQ NPs exhibited protective effects against L929 cells when induced with oxidative stress (200 μM H_2O_2), leading to preservation of cell mitochondrial potential levels up to 76 % of control and cell viability up to 78 % before and after incubation with CeO_2@PQQ NPs. The results indicate that CeO_2@PQQ NPs can be regarded as a novel hybrid nanosystem that exhibits mitochondrial-directed control of oxidative stress.

KEYWORDS nanoparticles, oxidative stress, reactive oxygen species, antioxidants, nanocrystalline cerium oxide, CeO_2, pyrroloquinoline quinone, PQQ, mitochondria

ACKNOWLEDGEMENTS This research was funded by the Russian Science Foundation, grant No. 22-63-00082. TEM studies were performed using TEM from the Simbioz Center for the Collective Use of Research Equipment of Institute of Biochemistry and Physiology of Plants and Microorganisms (IBPPM RAS).

FOR CITATION Zamyatina E.A., Goryacheva O.A., Popova N.R. Physicochemical properties and biological activity of novel cerium oxide nanoparticles modified with pyrroloquinoline quinone. *Nanosystems: Phys. Chem. Math.*, 2024, **15** (5), 683–692.

1. Introduction

Oxidative stress and mitochondrial dysfunction represent a significant link in the pathogenesis of numerous pathological conditions and the process of ageing [1–4]. Under normal conditions, mitochondria are responsible for the majority of free radical oxidation products generated by the electron transport chain and oxidative phosphorylation, and reactive oxygen species (ROS) are a normal component of numerous metabolic processes within cells [5, 6]. Nevertheless, dysfunctional mitochondria play an important role in the development of oxidative stress, and, as a result, become major targets for ROS [7, 8]. Mitochondrial DNA damage resulting from oxidative stress can lead to impaired energy metabolism and the development of a variety of mitochondrial diseases (Alzheimer's disease, diabetes, muscular dystrophy, cardiomyopathy, etc.) [9–12]. The probability of oxidative stress is contingent upon the level of ROS produced and their relative neutralization by the body's defensive mechanisms, which encompass a complex array of endogenous low molecular weight antioxidants (including superoxide dismutase, catalase, and glutathione peroxidase) [13–16]. When endogenous antioxidant systems are unable to effectively neutralize the increased generation of ROS, exogenous antioxidants can be introduced into biological systems to prevent the development of oxidative stress. The objective is to utilize mitochondrial-directed antioxidant systems to regulate ROS levels and maintain mitochondrial function, while ensuring high biocompatibility and catalytic activity. The utilization of both individual antioxidant compounds and the synthesis of novel combination therapies can be employed for this purpose.

Nanozymes are regarded as a promising platform for the development of new antioxidants that exhibit enhanced characteristics [17, 18]. Nanoparticles that have been functionalized with antioxidants or antioxidant enzymes have the ability to neutralize ROS in a more efficient manner than traditional antioxidants. This is achieved through the enhancement of intrinsic catalytic functions and the promotion of synergistic action with antioxidants [19].

Cerium oxide nanoparticles (CeO_2 NPs) are considered to have promising potential for use as a combined antioxidant due to their distinctive physicochemical properties. In nanoscale particles, the two oxidation states coexist on the nanoparticle's surface, thereby defining a dynamic redox switching process [20,21]. CeO_2 NPs are biocompatible nanozymes that exhibit a range of biomimetic activities, including superoxide dismutase, catalase, glutathione peroxidase, photolyase and phosphatase properties [22]. The mimesis of antioxidant enzymes depends on Ce^{+4}/Ce^{+3} redox switching on the nanoparticle's surface, which may enable them to act as autoregenerative free radical scavengers [23–28].

Pyrroloquinoline quinone (PQQ) is known for its high free radical neutralizing activity [29, 30]. Furthermore, recent studies have demonstrated that PQQ may exert a targeted effect on mitochondria, promoting their biogenesis and participating in the regulation of redox processes within the respiratory chain, maintaining the level of intracellular NAD^+ and stimulating the activity of NAD-dependent enzymes [31–33].

Despite the exceptional properties exhibited by CeO_2 NPs and PQQ, no previous works have demonstrated the properties of the combined action of these two components. In particular, the activity of CeO_2 NPs functionalized with redox-active quinones in biological systems has not been established. It is presumed that the modification of CeO_2 NPs with PQQ can provide a synergistic effect by combining both components in a single material and can therefore be considered as an innovative approach to combat oxidative stress. The nanoparticles exhibit dual functionality, they are capable of neutralizing ROS that cause oxidative stress and simultaneously protecting the mitochondrial function of biological systems.

The development of new nanoparticles allows for the enhancement of the properties of the individual components and for the delivery of a more effective and focused therapeutic intervention. PQQ was selected as an agent capable of synergizing with CeO_2, enhancing the antioxidant functions of CeO_2 and exerting a protective effect on mitochondria, which are the key compartment of ROS formation in the cell.

In this study, we synthesized CeO_2@PQQ NPs, studied the physicochemical properties of the nanoparticles, investigated their cytotoxicity on L929 cells, and examined the protective effects against 200 μM H_2O_2-induced oxidative stress.

2. Materials and methods

2.1. CeO_2@PQQ NPs synthesis

The following reagents were used for the synthesis of CeO_2@PQQ NPs: $CeCl_3 \cdot 7H_2O$ (purity 99 %, Alfa Aesar, USA), PQQ (purity 99 %, Xi'An Horlden Bio Industries Inc, China), KOH (purity $\geq$ 98 %, Lachema, Czech Republic), NH_4OH (25 %) (Dia-M, Russia). The nanoparticles were obtained via the precipitation method, which is described in brief below: PQQ was added to water and then mixed with a twofold excess of KOH. Subsequently, $CeCl_3 \cdot 7H_2O$ was added to the resulting solution, which was then stirred vigorously on a magnetic stirrer. The developed nanoparticles were then stabilized with 25 % NH_4OH in the requisite quantity until the pH of the solution reached a range of 7.2 – 7.6.

2.2. Characterization of CeO_2@PQQ NPs

The hydrodynamic size and zeta potential values were obtained via dynamic light scattering (DLS) and electrophoretic light scattering (ELS), respectively, using a BeNano Zeta particle size analyzer (BetterSize, Dandong, China). UV-Vis absorption and fluorescence spectra were measured in a quartz cuvette with an optical path length of 10 mm. Absorption spectra were obtained on a Shimadzu UV-1800 spectrophotometer (Shimadzu, Japan). Fluorimeter Cary Eclipse (Agilent Technologies, Australia) was used to obtain fluorescence spectra. Fourier Transform Infrared (FTIR) spectra were recorded from powder samples on a FT-801 FTIR spectrometer (Simex, Russia). To obtain powder, samples were dried in a freeze dryer (Labconco Corp, USA). The size and structural morphology of obtained NPs were observed using a transmission electron microscope (TEM) Libra 120 (Carl Zeiss, Oberkochen, Germany) and scanning electron microscopy (SEM) using a MIRA II LMU instrument (Tescan, Czech Republic) at an operating voltage of 20 kV.

2.3. Cell culture

Mouse fibroblasts (NCTC L929) were obtained from Theranostics and Nuclear Medicine Laboratory cryostorage (ITEB RAS, Pushchino, Russia). L929 cells were cultured in Dulbecco's Modified Eagle's Medium (DMEM)/F12 (1:1), containing 50 μg/mL of penicillin, 50 μg/mL of streptomycin, 1 % of L-glutamine and 10 % of fetal bovine serum (FBS) under 5 % CO_2 at 37 °C. The cells were seeded on 96-well plates at a density of 25000 cells/cm^2. After the cells had attached, the medium in the wells was replaced with fresh medium containing nanoparticles at concentrations of 0.1 – 100 μM. Cells in the control group were cultured in medium without added nanoparticles.

2.4. MTT assay

The determination of mitochondrial and cytoplasmic dehydrogenases activity in living cells was carried out using a MTT assay based on the reduction of the colorless tetrazolium salt (3-[4.5-dimethylthiazol-2-yl]-2.5-diphenyltetrazolium bromide, MTT, Sigma-Aldrich, USA). Briefly, CeO_2@PQQ NPs were added to cells growing in 96-well plates (for 24, 48 and 72 h at 37 °C in humid air (98 %) containing 5 % CO_2). 3 h prior to the end of the exposure period, the supernatant was removed, and MTT solution in phosphate-buffered saline (0.5 mg/mL, 100 μL/well) was added to the cells for 10 min.

Upon the completion of the exposure period, the supernatant was removed, and a lysis solution containing 0.1 % sodium do-decyl sulfate (Sigma-Aldrich, USA) solution in dimethyl sulfoxide was added. Plates were shaken for 10 min, placed on a microplate spectrophotometer Multiskan FC (Thermo Fisher, USA), and the absorbance was read colorimetrically at 570 nm. Each experiment was repeated three times, with five replications.

2.5. LIVE/DEAD assay

Cell viability after co-incubation with nanoparticles was assessed using a BioRad ZOE Fluorescent Cell Imager. Cells were seeded into 96-well plates and stained with Hoechst 33342 fluorescent dye (absorption – 350 nm, emission – 461 nm) and a propidium iodide (PI) dye (absorption – 493 nm, emission – 636 nm). The dyes were added to the DMEM/F12 without serum (1 μg/ml) and the plate was placed in a CO_2 incubator for 15 min. Images were captured after washing the cells with a phosphate-buffered saline. Five fields in each well for each cell group were examined. The number of cells (total cells/dead cells) was calculated using the ImageJ software.

2.6. Mitochondrial membrane potential assay

The mitochondrial membrane potential was measured by staining cells with TMRE (tetramethylrhodamine ethyl ester, ThermoFisher, USA) fluorescent dye followed by fluorescence microscopy analysis. After incubating with nanoparticles for 24 hours, the medium was replaced with TMRE solution in Hanks' buffer. The cells were subsequently photographed using a ZOE fluorescence imager. The fluorescence intensity of the TMRE, which is indicative of mitochondrial membrane potential levels in the cells, was quantified using ImageJ software. Three different areas on three separate microphotographs were analyzed for quantitative assessment.

2.7. Measurement of mitochondrial ROS production

For analysis of mitochondrial ROS, cells were treated with 1 μM MitoSOX (Invitrogen, USA) for 15 min and analyzed using a ZOE fluorescence imager. The fluorescence intensity of reactive oxygen species (ROS) in each of 100 randomly selected cells was quantified using ImageJ software. To ensure the accuracy of the scoring process, the data were scored and analyzed independently by two investigators.

2.8. Oxidative stress model in vitro

The protective action of CeO_2@PQQ NPs was analyzed using experimental model of oxidative stress, whereby the cells were treated with 200 μM H_2O_2 (30 %, Sigma-Aldrich, USA). In one case, nanoparticles were added to the cell culture, then 24 hours later the cells were treated with H_2O_2 for 60 min. In another case, the cells were immediately incubated with H_2O_2 for 60 min, after which the nanoparticles were added and the cells were incubated for 24 hours. At the end of the incubation period, cytotoxicity tests were performed, including the MTT test and the LIVE/DEAD test, and the level of mitochondrial status was examined by measuring the level of mitochondrial potential. All of the tests were carried out as described in the methodology above.

2.9. Statistical analysis

The data obtained from the MTT test, LIVE/DEAD test, measurement of mitochondrial potential level and mitochondrial ROS level were presented as mean $\pm$ standard deviation. The statistical analysis was performed using Welch's t-test. A p-value of less than 0.05 was considered to be statistically significant between the control and experimental groups.

3. Results and discussion

CeO_2@PQQ NPs were prepared using the precipitation method, the proposed schematic structure of which is shown in Fig. 1. To study the morphology and size of the obtained structures TEM images were analyzed (Fig. 2(D, E)). The obtained samples were compared with CeO_2 NPs (Fig. 2(A, B)), which have been previously obtained by our colleagues and have been well described [34]. From the image, it can be seen that the obtained samples are nanoparticles with the size ranging from 1.6 to 3.9 nm or aggregates of several nanoparticles. FTIR data (Fig. 2(G)) confirmed the similarity of the obtained structures with CeO_2 NPs. The sharpband peak centered at 500 cm^{-1}, which match to Ce–O stretching vibrations, confirmed the formation CeO_2 nanostructures [35].

The SEM and DLS data (Fig. 2(C, F, J)) differed from the TEM image analysis results. This can indicate the formation of complexes or a large layer of adsorbed organic molecules. Nanocluster formation can occur due to the fact that PQQ can bind to the Ñe atom on the surface of CeO_2 NPs in three ways via quinone carbonyl oxygen, pyridine nitrogen, and carboxylate [36]. The zeta potential of the obtained nanoparticles was found to be -38 mV (Fig. 2(K)), which is similar to the zeta potential values of classical citric acid-coated CeO_2 NPs with a zeta potential of around -30 mV [37]. This may indicate that the obtained nanoparticles possess high colloidal stability. PQQ is a multicharged anion, which gives the particles a negative charge, ammonia in turn provides ionization of PQQ and sol stability due to repulsion.

According to infrared spectroscopy, PQQ has a characteristic spectrum from 500 to 1790 cm^{-1} (Fig. 2(G)). The spectra of CeO_2@PQQ NPs showed a series of characteristic peaks of PQQ. Thus, 1116 cm^{-1} indicates C–H bond, 1393 cm^{-1}

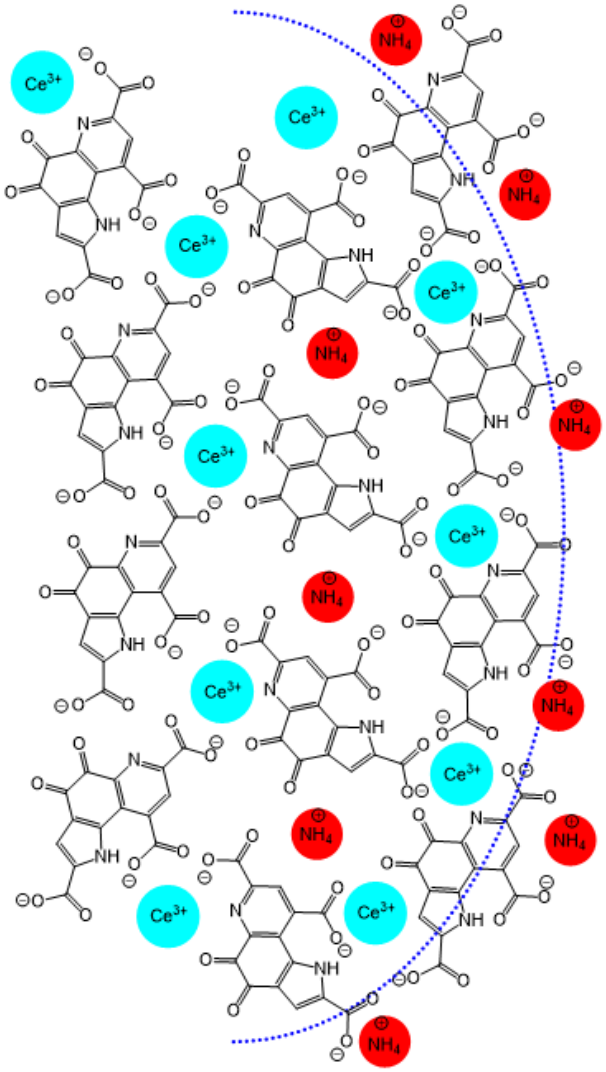

FIG. 1. Schematic representation of the proposed chemical structure of CeO_2@PQQ NPs. The blue line represents the conditional boundary of the nanoparticle

is characteristic for C–C bond in the aromatic ring [38] and 1543 cm^{-1} band indicates C–N [39] and 1505 cm^{-1} characteristic of the C=O stretching vibrations [40].

A spectrophotometric method was used to evaluate the sorption of PQQ on the surface of CeO_2 NPs. PQQ absorption spectrum is characterized by pronounced maxima at 248, 275 and 333 nm (Fig. 2(I)). During nanoparticles synthesis, the transition of PQQ into anion changed the shape of the spectrum and shifted the maxima. Thus, when the anion PQQ3- appeared in solution, the peak at 275 nm was significantly smoothed and the maximum at 333 nm is shifted to the longer wavelength region [41]. Upon sorption of PQQ on the surface of CeO_2 NPs, there was a significant change in the absorption spectrum of PQQ. The absorption maximum from 248 nm underwent a bathochromic shift to 257 nm. The maximum at 275 nm disappeared, while the peak of the maximum at 333 nm broadened and decreased relative to 257 nm. Similar changes in the absorption spectrum of PQQ were observed upon addition of Eu, another element from the lanthanide group [41]. PQQ has a characteristic fluorescence with a peak maximum at 480 nm (Fig. 2(H)) and the shape of the fluorescence spectrum did not change upon adsorption on the surface of CeO_2 NPs.

L929 mouse fibroblasts are a widely used cell culture for cytotoxicity studies and is frequently utilized as a standard subject for biocompatibility studies of nanomaterials [42]. The cytotoxicity of the CeO_2@PQQ NPs was evaluated using the MTT assay, which assesses the metabolic activity of cells by measuring the activity of cellular NAD(P)H-dependent oxidoreductases (Fig. 3(A)). The incubation of L929 cells with CeO_2@PQQ NPs for 24 – 72 hours at concentrations of 0.1 – 2 μM did not result in any significant cytotoxicity. Conversely, the values of metabolic activity exhibited a notable increase, reaching up to 112 %. This effect of increasing cell viability has been demonstrated in other studies involving CeO_2 NPs, where it is presumed that such values can be correlated with the number of mitochondria in cells and the participation of cytosolic enzymes [43]. However, in this study, this effect was only observed for the initial CeO_2@PQQ NPs investigated (0.1 – 2 μM), at which the differences between the control and the studied groups were not statistically

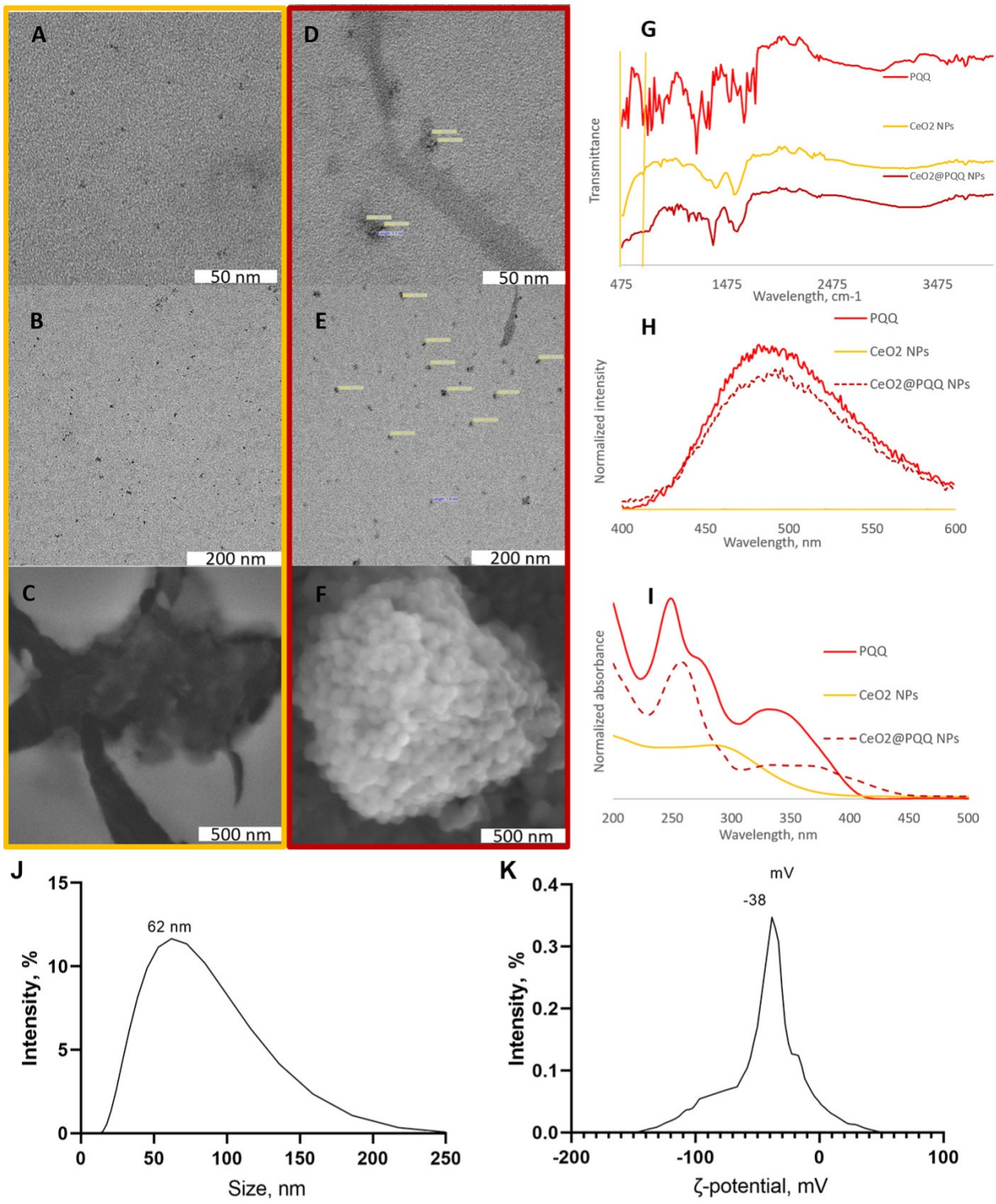

FIG. 2. Transmission electron microscopy images of CeO_2 NPs stabilized with citric acid (A, B) and CeO_2@PQQ NPs (D, E), scanning electron microscopy images of CeO_2 NPs stabilized with citric acid (C) and CeO_2@PQQ NPs (F), FTIR spectra (G), fluorescence spectra (H) and absorption spectra (I) of PQQ, CeO_2 NPs and CeO_2@PQQ NPs, hydrodynamic diameter distribution (J) and zeta potential distribution (K) of CeO_2@PQQ NPs

different. However, the viability of L929 decreased to 46 % when incubated with 10 μM CeO_2@PQQ NPs for 24 hours, but this value increased to 65 and 88 % after 48 and 72 hours of incubation, respectively. Incubation of the L929 cells with CeO_2@PQQ NPs at concentrations of 20 – 100 μM resulted in a significant reduction in cell metabolic activity. The incubation of L929 cells with CeO_2@PQQ NPs at concentrations of 20 – 100 μM resulted in a significant reduction in metabolic activity, with a decrease from 57 to 12 % being observed.

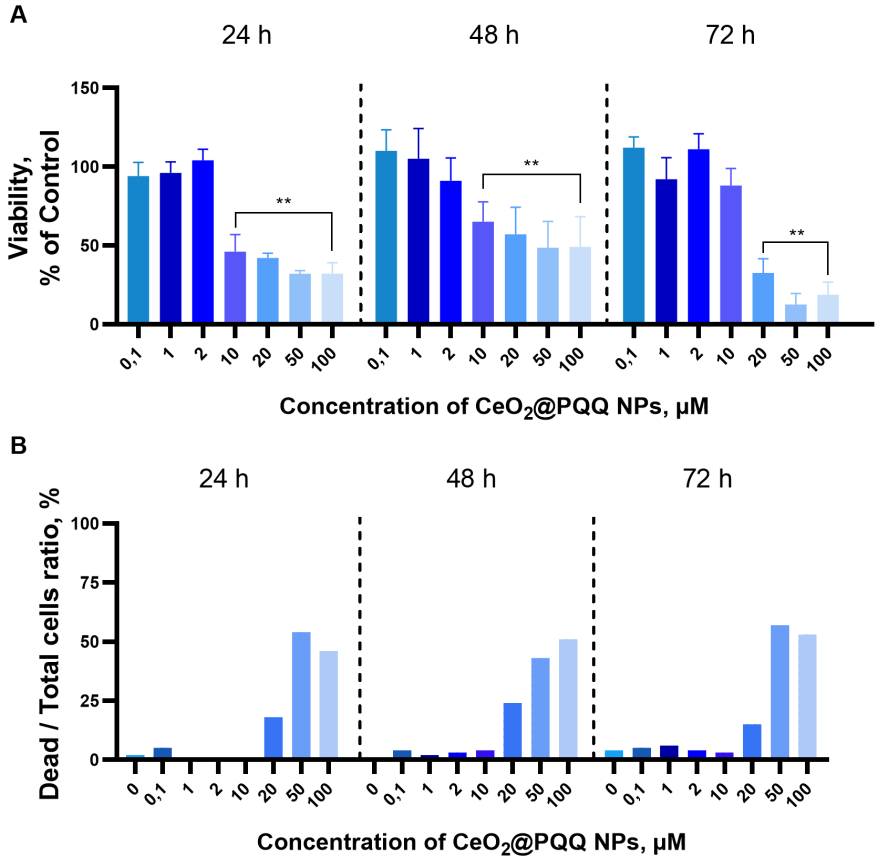

FIG. 3. MTT assay (A) and LIVE/DEAD test (B) results obtained on mouse fibroblasts (L929). The cells were incubated with CeO_2@PQQ NPs in concentrations 0.1 – 100 μM. The test was carried out after 24, 48, and 72 hours. Results are represented as a mean $\pm$ SD. The values of the metabolic activity of cells are shown as a percentage of the control. Statistical significance was assumed for P-values < 0.05: ($*P < 0.05$, $**P < 0.01$)

A LIVE/DEAD assay was used to visualize the distribution of live and dead cells of the L929. All cells were stained with Hoechst 33342 (blue fluorescence), while dead cells were stained with propidium iodide (PI) (red fluorescence). (Fig. 3(B)). A notable increase in the number of dead cells (approximately 25 %) was observed in the group with a CeO_2@PQQ NPs concentration of 20 μM. The number of dead cells exceeded 50 % when L929 was incubated with CeO_2@PQQ NPs at concentrations of 50 – 100 μM. Consequently, CeO_2@PQQ NPs at concentrations of 0.1 – 10 μM had no pronounced cytotoxic effect on L929, but at concentrations of 20 – 100 μM resulted in decreased metabolic activity and cell death.

Mitochondrial membrane potential was evaluated through assessment of the cationic dye tetramethylrhodamine (TMRE). The accumulation of TMRE within active mitochondria is due to the relative negative membrane potential of these organelles (Fig. 4(A)). The mitochondrial potential values of the cells were obtained following a 24-hour incubation period with CeO_2@PQQ NPs at a concentration range of 0.1 to 100 μM. It was demonstrated that a reduction in mitochondrial potential values was observed when CeO_2@PQQ NPs were incubated with concentrations of 20 – 100 μM, with a decrease of up to 75 % compared to the intact control.

The fluorescent dye MitoSOX is commonly used to detect ROS in mitochondria, particularly superoxide anions (Fig. 4(B)). Following the incubation of L929 cells with 1 – 100 μM CeO_2@PQQ NPs, the superoxide level exhibited no significant changes in comparison to the control. The results demonstrated that CeO_2@PQQ NPs at concentrations 1 – 10 μM had no significant impact on mitochondrial function.

The exposure of cell cultures to H_2O_2 is a widely employed method for the induction of oxidative stress [44, 45]. L929 cells were treated with H_2O_2 (200 μM, 60 min) prior to and subsequent to incubation with CeO_2@PQQ NPs. The viability of L929 cells incubated with CeO_2@PQQ NPs at concentrations of 0.1 – 10 μM was maintained at 63 – 78 %

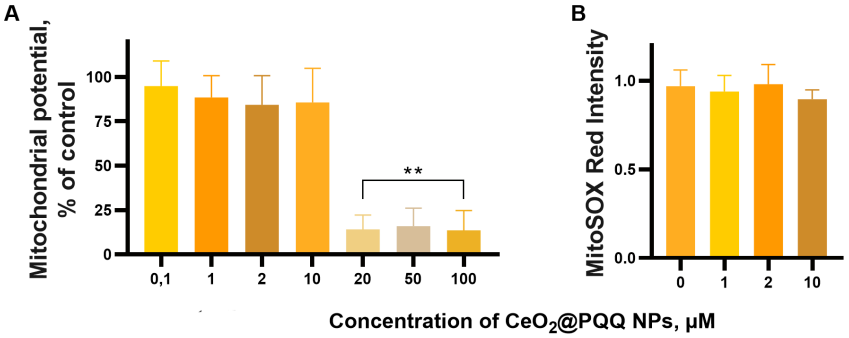

FIG. 4. Mitochondrial membrane potential (A) and mitochondrial ROS levels (B) results were obtained on L929 cells following 24-hour incubation with CeO_2@PQQ NPs at concentrations of 0.1 – 100 μM. Results are represented as a mean $\pm$ SD. The values of the mitochondrial potential of cells are shown as a percentage of the control. Statistical significance was assumed for P-values < 0.05: ($^*P < 0.05$, $^{**}P < 0.01$)

before and after incubation with nanoparticles, as determined by the MTT assay (Fig. 5). Meanwhile, concentrations of CeO_2@PQQ NPs in the range of 20 – 100 μM were found to negatively affect the metabolic activity of cells, reducing cell viability by up to 15 %. The results of the LIVE/DEAD test exhibited a comparable pattern: the number of dead cells in the concentration range of 0.1 – 10 μM CeO_2@PQQ NPs did not exceed 20 %, while 100 % of cells were observed to be dead in the range of 20 – 100 μM (Fig. 6).

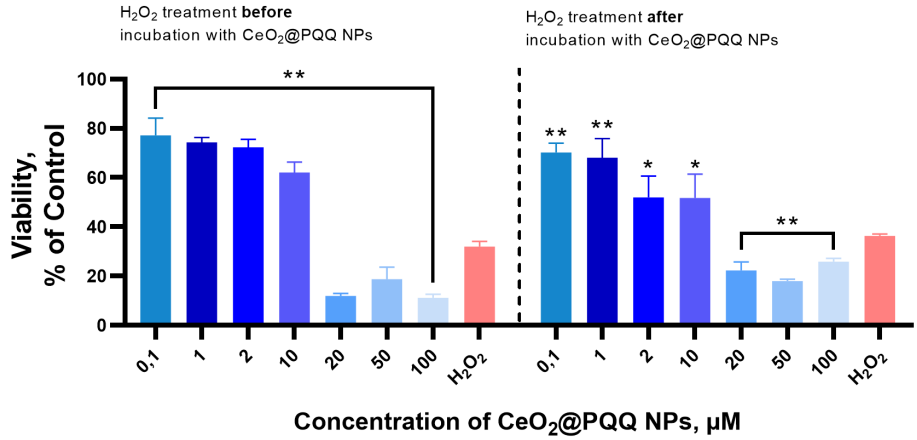

FIG. 5. MTT assay results obtained on mouse fibroblasts (L929). The cells were incubated with CeO_2@PQQ NPs in concentrations 0.1 – 100 μM before and after H_2O_2 treatment. The test was carried out after 24 hours. Results are represented as a mean $\pm$ SD. The values of the metabolic activity of cells are shown as a percentage of the control. Statistical significance was assumed for P-values < 0.05: ($^*P < 0.05$, $^{**}P < 0.01$)

According to TMRE fluorescence, after treatment of cells with H_2O_2, their mitochondrial potential decreased to 37 – 47 % (Fig. 7). Furthermore, following the incubation of cells in the presence of CeO_2@PQQ NPs, a concentration range of 0.1 – 100 μM, mitochondrial potential was maintained at 48 – 76 % of control levels. Upon the introduction of CeO_2@PQQ NPs subsequent to H_2O_2 treatment, effective concentrations capable of inhibiting mitochondrial membrane depolarization were observed to range from 0.1 to 2 μM.

It can be postulated that the CeO_2@PQQ NPs obtained may result in the reduction of H_2O_2-induced oxidative stress in L929 cells. The depolarization of the mitochondrial membrane can be indicative of severe mitochondrial damage, given that mitochondria are a major source of ROS within cells [46]. It is probable that the modification of CeO_2NPs with PQQ will not only enhance their catalytic activity for ROS neutralizing, but also have a beneficial impact on mitochondrial function [33]. The presence of the redox-active cerium ion may potentially accelerate redox reactions involving PQQ. Upon induction of oxidative stress by the incubation of L929 cells with H_2O_2 at a concentration of 200 μM, the nanoparticles under investigation exhibited a preservation of cell viability at 63 – 78 % both before and after nanoparticle application, and of mitochondrial potential at 48 – 76 % of control values across concentrations ranging from 0.1 to 10 μM.

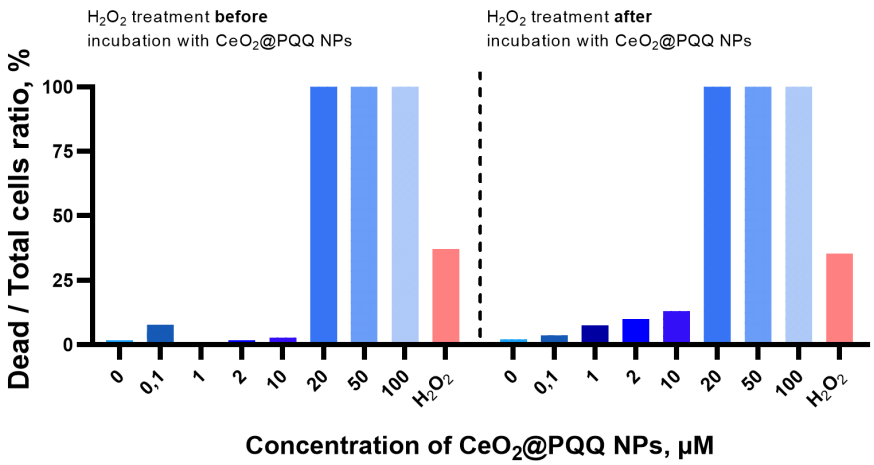

FIG. 6. LIVE/DEAD test results obtained on mouse fibroblasts (L929). The cells were incubated with CeO_2@PQQ NPs in concentrations 0.1 – 100 μM before and after H_2O_2 treatment. The test was carried out after 24 hours. Results are represented as a mean $\pm$ SD. The values of the metabolic activity of cells are shown as a percentage of the control. Statistical significance was assumed for P-values < 0.05: ($*P < 0.05$, $**P < 0.01$)

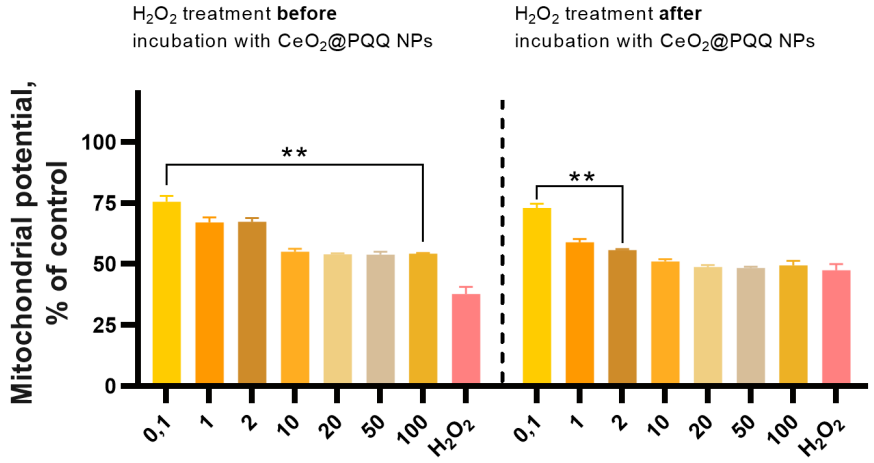

FIG. 7. Mitochondrial membrane potential results were obtained on L929 cells following 24-hour incubation with CeO_2@PQQ NPs at concentrations of 0.1 – 100 μM before and after H_2O_2 treatment. Results are represented as a mean $\pm$ SD. The values of the mitochondrial potential of cells are shown as a percentage of the control. Statistical significance was assumed for P-values < 0.05: ($*P < 0.05$, $**P < 0.01$)

4. Conclusions

CeO_2@PQQ NPs were successfully obtained by precipitation method. The nanoparticles were characterized by a variety of techniques, including TEM, SEM, DLS, ELS, FTIR and UV-Vis spectroscopy. The morphological study using TEM and SEM revealed that the majority of CeO_2@PQQ NPs exhibited a size range of up to 3.9 nm. The results of the FTIR confirmed the formation of CeO_2 structures and demonstrated the presence of PQQ on the surface of CeO_2 NPs. The results of the DLS analysis indicate that CeO_2@PQQ NPs have an average diameter of 62 nm in solution. The ELS measurements yielded zeta potential of -38 mV, which is indicative of CeO_2@PQQ NPs sufficient colloidal stability. At concentrations up to 20 μM, no reduction in the mitochondrial potential values of L929 was observed. When oxidative stress was induced by treating the L929 cell line with H_2O_2 at a concentration of 200 μM, the nanoparticles under investigation demonstrated the capacity to preserve cell viability at 63 – 78 % before and after nanoparticle addition, as well as to preserve mitochondrial potential at 48 – 76 % of control values at concentrations of 0.1 – 10 μM. Consequently, CeO_2@PQQ NPs may offer new opportunities to combat oxidative stress through their synergistic properties.

References

[1] Yang S., Lian G. ROS and diseases: role in metabolism and energy supply. *Mol Cell Biochem*, 2020, **467**, P. 1–12.

[2] Ott M., Gogvadze V., Orrenius S., Zhivotovsky B. Mitochondria, oxidative stress and cell death. *Apoptosis*, 2007, **12**, P. 913–922.

[3] Jomova K., Raptova R., Alomar S.Y., Alwasel S.H., Nepovimova E., Kuca K., Valko M. Reactive oxygen species, toxicity, oxidative stress, and antioxidants: chronic diseases and aging. *Arch Toxicol*, 2023, **97**, P. 2499–2574.

[4] Kowalczyk P., Sulejczak D., Kleczkowska P., Bukowska-Ośko I., Kucia M., Popiel M., Wietrak E., Kramkowski K., Wrzosek K., Kaczyńska K. Mitochondrial oxidative stress—A causative factor and therapeutic target in many diseases. *IJMS*, 2021, **22**, 13384.

[5] Liu Y., Fiskum G., Schubert D. Generation of reactive oxygen species by the mitochondrial electron transport chain. *J. of Neurochemistry*, 2002, **80**, P. 780–787.

[6] Lennicke C., Cochemé H.M. Redox metabolism: ROS as specific molecular regulators of cell signaling and function. *Molecular Cell*, 2021, **81**, P. 3691–3707.

[7] Newmeyer D.D., Ferguson-Miller S. Mitochondria. *Cell*, 2003, **112**, P. 481–490.

[8] Mailloux R.J. An Update on Mitochondrial Reactive Oxygen Species Production. *Antioxidants*, 2020, **9**, 472.

[9] Filograna R., Mennuni M., Alsina D., Larsson N. Mitochondrial DNA copy number in human disease: the more the better? *FEBS Letters*, 2021, **595**, P. 976–1002.

[10] Wei W., Chinnery P.F. Inheritance of mitochondrial DNA in humans: implications for rare and common diseases. *J. Intern. Med.*, 2020, **287**, P. 634–644.

[11] Pereira C.V., Gitschlag B.L., Patel M.R. Cellular mechanisms of mtDNA heteroplasmy dynamics. *Critical Reviews in Biochemistry and Molecular Biology*, 2021, **56**, P. 510–525.

[12] Mustafa M.F., Fakurazi S., Abdullah M.A., Maniam S. Pathogenic Mitochondria DNA Mutations: Current Detection Tools and Interventions. *Genes*, 2020, **11**, 192.

[13] Pisoschi A.M., Pop A. The role of antioxidants in the chemistry of oxidative stress: A review. *European J. of Medicinal Chemistry*, 2015, **97**, P. 55–74.

[14] Elsayed Azab A., Adwas A.A., Ibrahim Elsayed A.S., Adwas A.A., Ibrahim Elsayed A.S., Quwaydir F.A. Oxidative stress and antioxidant mechanisms in human body. *JABB*, 2019, **6**, P. 43–47.

[15] Nandi A., Yan L.-J., Jana C.K., Das N. Role of Catalase in Oxidative Stress- and Age-Associated Degenerative Diseases. *Oxidative Medicine and Cellular Longevity*, 2019, **2019**, P. 1–19.

[16] Ighodaro O.M., Akinloye O.A. First line defence antioxidants-superoxide dismutase (SOD), catalase (CAT) and glutathione peroxidase (GPX): Their fundamental role in the entire antioxidant defence grid. *Alexandria J. of Medicine*, 2018, **54**, P. 287–293.

[17] Li C.-W., Li L.-L., Chen S., Zhang J.-X., Lu W.-L. Antioxidant nanotherapies for the treatment of inflammatory diseases. *Front. Bioeng. Biotechnol.*, 2020, **8**, 200.

[18] Kim Y.G., Lee Y., Lee N., Soh M., Kim D., Hyeon T. Ceria-based therapeutic antioxidants for biomedical applications. *Advanced Materials*, 2024, **36**, 2210819.

[19] Khalil I., Yehye W.A., Etxeberria A.E., Alhadi A.A., Dezfooli S.M., Julkapli N.B.M., Basirun W.J., Seyfoddin A. Nanoantioxidants: Recent trends in antioxidant delivery applications. *Antioxidants*, 2019, **9**, 24.

[20] Celardo I., Pedersen J.Z., Traversa E., Ghibelli L. Pharmacological potential of cerium oxide nanoparticles. *Nanoscale*, 2011, **3**, 1411.

[21] Popov A.L., Andreeva V.V., Khohlov N.V., Kamenskikh K.A., Gavrilyuk V.B., Ivanov V.K. Comprehensive cytotoxicity analysis of polysaccharide hydrogel modified with cerium oxide nanoparticles for wound healing application. *Nanosystems: Phys. Chem. Math.*, 2021, **12**, P. 329–335.

[22] Li F., Yang L., Zou L., Wu Y., Hu C., He J., Yang X. Decreasing crystallinity is beneficial to the superoxide dismutase-like activity of ceria nanoparticles. *ChemNanoMat*, 2022, **8**, e202100466.

[23] Shcherbakov A.B., Reukov V.V., Yakimansky A.V., Krasnopeeva E.L., Ivanova O.S., Popov A.L., Ivanov V.K. CeO_2 Nanoparticle-containing polymers for biomedical applications: A Review. *Polymers*, 2021, **13**, 924.

[24] Filippova A.D., Baranchikov A.E., Ivanov V.K. Enzyme-like activity of cerium dioxide colloidal solutions stabilized with L-Malic acid. *Colloid J.*, 2023, **85**, P. 782–794.

[25] Ge X., Cao Z., Chu L. The antioxidant effect of the metal and metal-oxide nanoparticles. *Antioxidants*, 2022, **11**, 791.

[26] Corsi F., Deidda Tarquini G., Urbani M., Bejarano I., Traversa E., Ghibelli L. The impressive anti-inflammatory activity of cerium oxide nanoparticles: more than redox? *Nanomaterials*, 2023, **13**, 2803.

[27] Sozarukova M.M., Kozlova T.O., Beshkareva T.S., Popov A.L., Kolmanovich D.D., Vinnik D.A., Ivanova O.S., Lukashin A.V., Baranchikov A.E., Ivanov V.K. Gadolinium Doping Modulates the Enzyme-like Activity and Radical-Scavenging Properties of CeO_2 Nanoparticles. *Nanomaterials*, 2024, **14**, 769.

[28] Chukavin N.N., Filippova K.O., Ermakov A.M., Karmanova E.E., Popova N.R., Anikina V.A., Ivanova O.S., Ivanov V.K., Popov A.L. Redox-active cerium fluoride nanoparticles selectively modulate cellular response against X-ray irradiation In Vitro. *Biomedicines*, 2023, **12**, 11.

[29] Akagawa M., Nakano M., Ikemoto K. Recent progress in studies on the health benefits of pyrroloquinoline quinone. *Bioscience, Biotechnology, and Biochemistry*, 2016, **80**, P. 13–22.

[30] Ikemoto K., Mohamad Ishak N.S., Akagawa M. The effects of pyrroloquinoline quinone disodium salt on brain function and physiological processes. *J. Med. Invest.*, 2024, **71**, P. 23–28.

[31] Mohamad Ishak N.S., Ikemoto K. Pyrroloquinoline-quinone to reduce fat accumulation and ameliorate obesity progression. *Front. Mol. Biosci.*, 2023, **10**, 1200025.

[32] Banerjee R., Purhonen J., Kallijärvi J. The mitochondrial coenzyme Q junction and complex III: biochemistry and pathophysiology. *The FEBS Journal*, 2022, **289**, P. 6936–6958.

[33] Jonscher K.R., Chowanadisai W., Rucker R.B. Pyrroloquinoline-quinone is more than an antioxidant: A vitamin-like accessory factor important in health and disease prevention. *Biomolecules*, 2021, **11**, 1441.

[34] Popov A.L., Popova N.R., Selezneva I.I., Akkizov A.Y., Ivanov V.K. Cerium oxide nanoparticles stimulate proliferation of primary mouse embryonic fibroblasts in vitro. *Materials Science and Engineering: C*, 2016, **68**, P. 406–413.

[35] Parimi D., Sundararajan V., Sadak O., Gunasekaran S., Mohideen S.S., Sundaramurthy A. Synthesis of positively and negatively charged CeO_2 nanoparticles: Investigation of the role of surface charge on growth and development of Drosophila melanogaster. *ACS Omega*, 2019, **4**, P. 104–113.

[36] Itoh S., Kawakami H., Fukuzumi S. Development of the active site model for calcium-containing quinoprotein alcohol dehydrogenases. *J. of Molecular Catalysis B: Enzymatic*, 2000, **8**, P. 85–94.

[37] Tsai Y.-Y., Oca-Cossio J., Agering K., Simpson N.E., Atkinson M.A., Wasserfall C.H., Constantinidis I., Sigmund W. Novel synthesis of cerium oxide nanoparticles for free radical scavenging. *Nanomedicine*, 2007, **2**, P. 325–332.

[38] Wang L., Roitberg A., Meuse C., Gaigalas A.K. Raman and FTIR spectroscopies of fluorescein in solutions. *Spectrochimica Acta Part A: Molecular and Biomolecular Spectroscopy*, 2001, **57**, P. 1781–1791.
[39] Smith B.C. Infrared spectroscopy of polymers XII: Polyaramids and slip agents. *Spectroscopy*, 2023, **38** (5), P. 16–18.
[40] Ibrahim S., Rezk M.Y., Ismail M., Abdelrahman T., Sharkawy M., Abdellatif A., Allam N.K. Coaxial nanofibers outperform uniaxial nanofibers for the loading and release of pyrroloquinoline quinone (PQQ) for biomedical applications. *Nanoscale Adv.*, 2020, **2**, P. 3341–3349.
[41] Danaf N.A., Kretzschmar J., Jahn B., Singer H., Pol A., Op Den Camp H.J.M., Steudtner R., Lamb D.C., Drobot B., Daumann L.J. Studies of pyrroloquinoline quinone species in solution and in lanthanide-dependent methanol dehydrogenases. *Phys. Chem. Chem. Phys.*, 2022, **24**, P. 15397–15405.
[42] Ray R.S., Agrawal N., Sharma A., Hans R.K. Use of L-929 cell line for phototoxicity assessment. *Toxicology in Vitro*, 2008, **22**, P. 1775–1781.
[43] Tumkur P.P., Gunasekaran N.K., Lamani B.R., Nazario Bayon N., Prabhakaran K., Hall J.C., Ramesh G.T. Cerium oxide nanoparticles: synthesis and characterization for biosafe applications. *Nanomanufacturing*, 2021, **1**, P. 176–189.
[44] Goffart S., Tikkanen P., Michell C., Wilson T., Pohjoismäki J.L.O. The type and source of reactive oxygen species influences the outcome of oxidative stress in cultured cells. *Cells*, 2021, **10**, 1075.
[45] Ransy C., Vaz C., Lombès A., Bouillaud F. Use of H_2O_2 to cause oxidative stress, the catalase issue. *IJMS*, 2020, **21**, 9149.
[46] He K., Nukada H., Urakami T., Murphy M.P. Antioxidant and pro-oxidant properties of pyrroloquinoline quinone (PQQ): implications for its function in biological systems. *Biochemical Pharmacology*, 2003, **65**, P. 67–74.

Submitted 28 August 2024; accepted 26 September 2024

Information about the authors:

Elizaveta A. Zamyatina – Institute of Theoretical and Experimental Biophysics of the Russian Academy of Sciences, Institutskaya str., 3, Pushchino, 142290, Russia; ORCID 0000-0002-1275-565X; sonyoru162@gmail.com

Olga A. Goryacheva – Saratov State University named after N. G. Chernyshevsky, Chemistry Institute, Astrakhanskaya 83, Saratov, 410012, Russia; ORCID 0000-0002-0910-7694; Olga.goryacheva.93@mail.ru

Nelli R. Popova – Institute of Theoretical and Experimental Biophysics of the Russian Academy of Sciences, Institutskaya str., 3, Pushchino, 142290, Russia; ORCID 0000-0002-0982-6349; nellipopovaran@gmail.com

Conflict of interest: the authors declare no conflict of interest.